No. 1C-a62 $PbTiO_3$–$PbZrO_3$

See also No. 1C-a63 for electromechanical properties of $Pb(Zr_xTi_{1-x})O_3$ with x = 0.5...0.6.

1a	Ferro- and antiferroelectric phase transitions in the $PbTiO_3$–$PbZrO_3$ system were reported in 1952 by Shirane et al.	52Shi1
b	Phase diagram: Figs. 1C-a62-001...1C-a62-005; Table 1C-a62-001; see also	77Han, 83Bar, 85Han
	Phases: F_α, $F_{\alpha LT}$, $F_{\alpha HT}$: ferroelectric rhombohedral, $F_{\beta:}$ ferroelectric tetragonal, A_α: antiferroelectric orthorhombic, $A_{\beta:}$ antiferroelectric tetragonal, P: paraelectric cubic.	
	Space group: R3c – C_{3v}^6 in $F_{\alpha LT}$ [a]), R3m – C_{3v}^5 in $F_{\alpha HT}$ [a]), P4mm – C_{4v}^1 in F_β [b]), Pba2 – C_{2v}^8 in A_α [b]), Pm3m – O_h^1 in P [b]).	[a]) 69Mic [b]) 53Shi
2a	Phase diagram including liquid phase: Fig. 1C-a62-006.	
	Crystal growth: about flux method, see	62Ike, 64Fus, 67Fus, 69Tsu
	about hydrothermal method, see	71Bar
	Distribution curve [composition diagram (c_{solid} vs. c_{liquid}) for KF–PbF_2–$Pb_3(PO_4)_2$ flux]: Fig. 1C-a62-007.	
	Vapor pressure of PbO: Fig. 1C-a62-008.	
3a	Lattice parameter: Fig. 1C-a62-009, Fig. 1C-a62-010; see also	84Kut
b	Crystal structure ($Pb(Zr_{0.9}Ti_{0.1})O_3$): Table 1C-a62-002, Table 1C-a62-003; Figs. 1C-a62-011...1C-a62-013; see also	80Ami, 83Ito
4	Thermal distortion: Fig. 1C-a62-014, Fig. 1C-a62-015; see also	52Shi2, 52Shi3, 62Bar, 74Cla
5a	Dielectric constant:	
	crystals: Figs. 1C-a62-016...1C-a62-018;	
	ceramics: Fig. 1C-a62-019, Fig. 1C-a62-020.	
	Low temperature: Fig. 1C-a62-021.	
	Frequency dependence: Fig. 1C-a62-022.	
	Effect of electric field bias: Fig. 1C-a62-023.	
	Pressure effect: Figs. 1C-a62-024...1C-a62-026.	
c	Spontaneous polarization: Figs. 1C-a62-027...1C-a62-031.	
d	Pyroelectric effect: Fig. 1C-a62-032, Fig. 1C-a62-033; Table 1C-a62-004.	
6a	Specific heat: Fig. 1C-a62-034.	
	Transition heat: Table 1C-a62-005.	
7a	Piezoelectricity: Fig. 1C-a62-035.	
b	Electrostriction: Fig. 1C-a62-036; see also	84Zor
	Electromechanical properties: see also No. 1C-a63	
9a	Birefringence: Fig. 1C-a62-037.	

10a	Raman scattering: Figs. 1C-a62-038...1C-a62-040; see also	74Mer, 75Mer, 76Mer
11	Electrical conductivity: Fig. 1C-a62-041, Fig. 1C-a62-042. Thermoelectric effect: Fig. 1C-a62-043.	
13b	Electron paramagnetic resonance: see	90Gli, 92Byk, 93War
c	Mössbauer effect: see	74Ede
15a	Observation of domains: see	85Cha, 85Ngy, 90Ekn, 92Hat
16	Radiation damage effect: see Thin film: see	65Glo 79Ham1, 79Ham2, 79Cas, 83Fuk, 84Fuk, 85FuS, 94Als

Table 1C-a62-001. $Pb(Ti_{1-x}Zr_x)O_3$. Effect of pressure on phase transition [86Pol].

$PbZrO_3$ [wt%]	$d\Theta/dp$ (rhombohedral F to cubic P)	Coordinates of triple point		$d\Theta/dp$ (AF_{tet}–P_{cub})	Coordinates of triple point	
	[K GPa^{-1}]	p [GPa]	T [°C]	[K GPa^{-1}]	p [GPa]	T [°C]
98	–80	0.1	220	45	0.66	245
96	–80	0.18	218	52	0.66	245
95	–31	0.24	219	90	–	–
94	–40	0.28	219	80	0.60	245
92	–40	0.38	220	80	0.60	235
90	–80	0.41	209	60	0.60	220
88	–80	0.45	210	60	0.60	219
86	–80	0.64	214	–	–	–
70	–	–	–	–	–	–
65	–	–	–	–	–	–
60	–	–	–	–	–	–
56	–	–	–	–	–	–
50	–	–	–	–	–	–

$PbZrO_3$ [wt%]	$d\Theta/dp$ [K GPa^{-1}]	$d\Theta/dp$ [K GPa^{-1}]				p [GPa] (20°C)		Coordinates of triple point	
	region of high pressure	AF_{orth}–AF_{tet}	F_{rh}^{LT}–F_{rh}^{HT}	F_{orth}–AF_{tet}	non-F–P_{cub}	F_{orth}–non-F	non-F–P_{cub}	p [GPa]	T [°C]
98	130	55	–	–	–	–	–	–	–
96	107	60	–	–	–	–	–	–	–
95	90	60	–	–	–	–	–	–	–
94	37	60	–	–	–	–	–	–	–
92	37	60	–	–	–	–	–	–	–
90	33	60	110	–	–	–	–	–	–
88	18	60	150	–	–	–	–	–	–
86	17	–	150	–	–	–	–	–	–
70	–	–	–	–140	–67	3.2	4.0	2.4	150
65	–	–	–	–	–	3.8	6.2	–	–
60	–	–	–	–140	–40	4.0	7.2	2.8	210
56	–	–	–	–	–	4.3	7.6	–	–
50	–	–	–	–110	–40	4.8	8.4	2.8	235

Table 1C-a62-002. $Pb(Zr_{0.9}Ti_{0.1})O_3$. Atomic position parameters refined by powder profile analysis [78Gla]. Parameters *s* and *t* measure the fractional displacements of PbO and Zr/Ti, respectively, along the three-fold axis, and *d* and *e* describe the distortion and rotation of an octahedron. Based on the hexagonal cell (a_h, c_h), atomic position parameters are Pb: (0, 0, 1/4 + *s*), Zr/Ti: (0, 0, *t*), O: (1/6 − 2*e* − 2*d*, 1/3 − 4 *d*, 1/12). (The angle of tilt ω is given by $\tan\omega = 4\sqrt{3}\,e$.) Anisotropic temperature factors are also determined. See original paper.

T [°C]	25	60	100	150	200	235	300
Phase	$F_{\alpha LT}$		$F_{\alpha HT}$				P
Space group	$R3c–C_{3v}^6$		$R3m–C_{3v}^5$				$Pm3m–O_h^1$
a_h [Å]	5.8412	5.8434	5.8479	5.8510	5.8543	5.8564	
c_h [Å]	14.4122	14.4178	14.4239	14.4222	14.4115	14.3951	
a_{pc} [Å]	4.1404	4.1420	4.1447	4.1460	4.1465	4.1459	4.1449
α [°]	89.722	89.722	89.735	89.760	89.810	89.867	90.000
s [a])	0.0316(8)	0.0307(8)	0.0266(11)	0.0257(12)	0.0183(11)	0.0146(29)	
t [a])	0.0114(11)	0.0112(10)	0.0095(16)	0.0077(16)	0.0072(13)	0.0021(47)	
d	–0.0029(3)	–0.0023(3)	–0.0021(4)	–0.0011(11)	–0.0009(4)	–0.0007(9)	
e [a])	0.0137(5)	0.0122(6)					
ω [°] [a])	5.42(20)	4.83(24)					
Number of parameters	25	25	22	22	22	22	12
Number of reflections	80	85	56	59	50	59	21
R_{nuc} [%]	6.33	6.21	5.91	7.06	6.25	5.00	5.68
R_{prof} [%]	11.75	13.93	13.26	17.15	13.26	16.28	15.51
R_{exp} [%]	5.06	6.18	5.70	9.60	4.86	6.08	4.71
Number of counts in pseudocubic 200 reflection	17900	26000	25900	10000 [b])	30300	25400	33700

$R_{nuc} = 100\Sigma|I(\text{obs})–I(\text{calc})| / \Sigma I(\text{obs})$

$R_{prof} = 100\Sigma|y(\text{obs})–y(\text{calc})| / \Sigma|y(\text{obs})|$

$R_{exp} = 100[(N–P) / \Sigma wy(\text{obs})^2]^{-1/2}$

I(obs), *I*(calc) = observed and calculated integrated intensity of each reflection.

y(obs), *y*(calc) = observed and calculated profile data point.

w = weight allotted to each data point.

[a]) [69Mic]: *s* = 0.022(2), *t* = 0.006(2), *e* = 0.019(2), ω = 7.5(6)°.

[b]) The low count with this run was because the measurements were carried out near the end of the reactor cycle and when the monitor count rate was at its lowest.

Table 1C-a62-003. $Pb(Zr_{0.9}Ti_{0.1})O_3$. Structural parameters [83Ito]. Atomic positions are defined as Pb: (0, 0, 1/4 + *s*), Zr/Ti: (0, 0, *t*), O: (1/6 − 2*e* − 2*d*, 1/3 − 4 *d*, 1/12). a_h and c_h are hexagonal lattice constants obtained from X-ray measurements. B_i is isotropic temperature factor of each atom obtained from neutron data (see Eq. (e) in Introduction). For definitions of *s*, *t*, *d* and *e*, see Table 1C-a62-002.

a_h	5.841 Å	B_{Pb}	1.75(5) Å^2
c_h	14.416 Å	$B_{Zr/Ti}$	0.19(4) Å^2
s	0.0342(2)	B_O	0.91(2) Å^2
t	0.0151(2)	R_B(XD)	4.08%
d	–0.0037(1)	R_P(XD)	10.63%
e	0.0144(2)	R_B(ND)	3.72%
		R_P(ND)	7.59%

$R_B = \Sigma|I(\text{obs})-(1/k)I(\text{cal})| / \Sigma I(\text{obs})$

$R_p = \Sigma|Y(\text{obs})-(1/k)Y(\text{cal})| / \Sigma Y(\text{obs})$

I, *Y*, and *k*: integrated intensity for Bragg peaks, diffraction intensity at each data point, and scale factor, respectively.

Table 1C-a62-004. $Pb(Ti_{1-x}Zr_x)O_3$ (ceramics). Dielectric constant, loss and pyroelectric figure of merit [73Lan]. With additive of 0.3 wt % U_3O_8.

x	ρ	κ (f = 1 kHz)		tan δ (f = 1 kHz)	F.M.$_{R_I}$	F.M.$_{R_V}$
	[$\cdot 10^3$ kgm^{-3}]	(unpoled)	(poled)		[$\cdot 10^{-11}$ CmJ^{-1}]	[$\cdot 10^{-13}$ CmJ^{-1}]
0.74	7.60	490	340	0.010	10.6	32.0
0.78	7.53	490	310	0.012	10.8	34.8
0.82	7.47	480	310	0.013	10.7	34.7
0.86	7.41	440	270	0.022	10.5	38.1
0.90	7.40	430	270	0.023	10.3	39.1
0.92	7.35	600	230	0.016	10.2	44.6
0.928	7.21	590	220	0.013	10.4	46.4
0.936	7.31	580	230	0.011	10.8	48.8
0.940	7.23	360	220	0.030	11.2	48.1
0.944	7.22	570	220	0.012	12.1	53.5
0.952	7.15	540	230	0.017	8.0	35.0
0.960	7.12	340	200	0.013	1.6	7.5
0.980	6.98	140	140	0.008	0	0

F.M.$_{R_I}$ (= P/ρ_{Cp}): Figure of merit for current responsivity.

F.M.$_{R_V}$ (= $P/\rho_{Cp}\kappa$): Figure of merit for voltage responsivity.

Table 1C-a62-005. $Pb(Zr_{1-x}Ti_x)O_3$. Transition heat and entropy [53Saw]. It is assumed that the free energy decreases with the rate of $dS(d\Theta/dx)$ with increasing x.

Kind of the phase change	Θ [°C]	ΔQ_m [J mol^{-1}]	ΔS_m [J mol^{-1}K^{-1}]	$d\Theta/dx$	$dS(d\Theta/dx)$
$A_\alpha \rightarrow P$	230>*T*>225	1670	3.3	–	(–5.8)
$A_\alpha \rightarrow A_\beta$	225	460	0.92	–16	–3.5
$A_\beta \rightarrow P$	230	1210	2.42	–4	–2.3
$A_\alpha \rightarrow F_\alpha$	240	–	–	–19	–
$F_\alpha \rightarrow P$	217	1050	2.13	+1.0	+0.5
$A_\beta \rightarrow F_\alpha$		170	0.33		

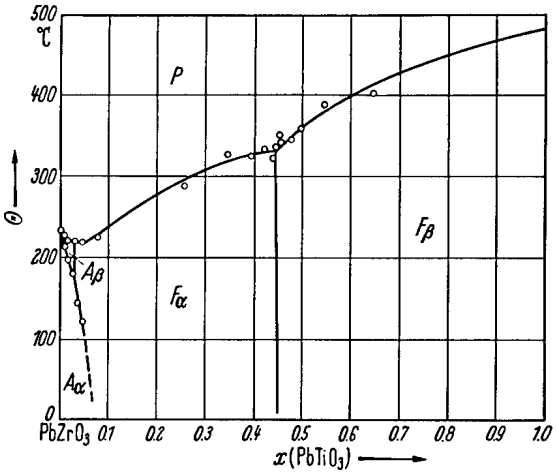

Fig. 1C-a62-001. $Pb(Zr_{1-x}Ti_x)O_3$. Θ vs. x [53Saw]. Phases: F_α: ferroelectric rhombohedral, F_β: ferroelctric tetragonal, A_α: antiferroelectric orthorhombic, A_β: antiferroelectric tetragonal, P: paraelectric cubic.

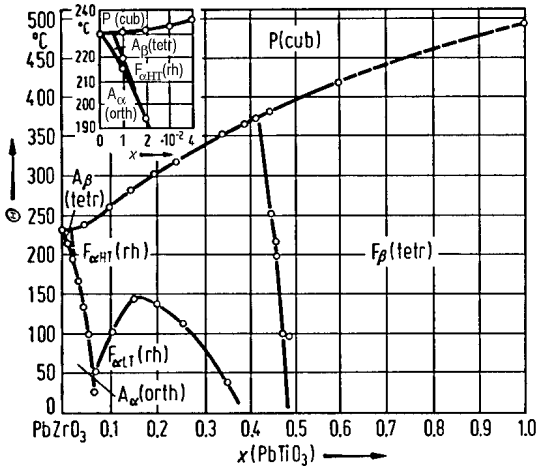

Fig. 1C-a62-002. $Pb(Zr_{1-x}Ti_x)O_3$. Θ vs. x [66Ber]. For explanations of phase symbols see subsection 1b of No. 1C-a62.

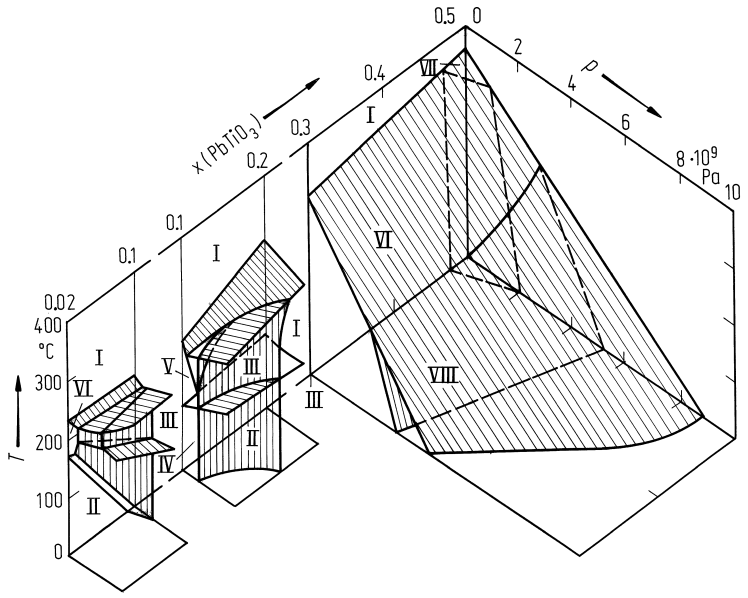

Fig. 1C-a62-003. $Pb(Zr_{1-x}Ti_x)O_3$. *T*–*p*–x phase diagram [86Pol]. Phases: I: P, II: A_α, III: A_β , IV: $F_{\alpha LT}$, V: $F_{\alpha HT}$, VI: F_α, VII: F_β , VIII: nonferroelectric.

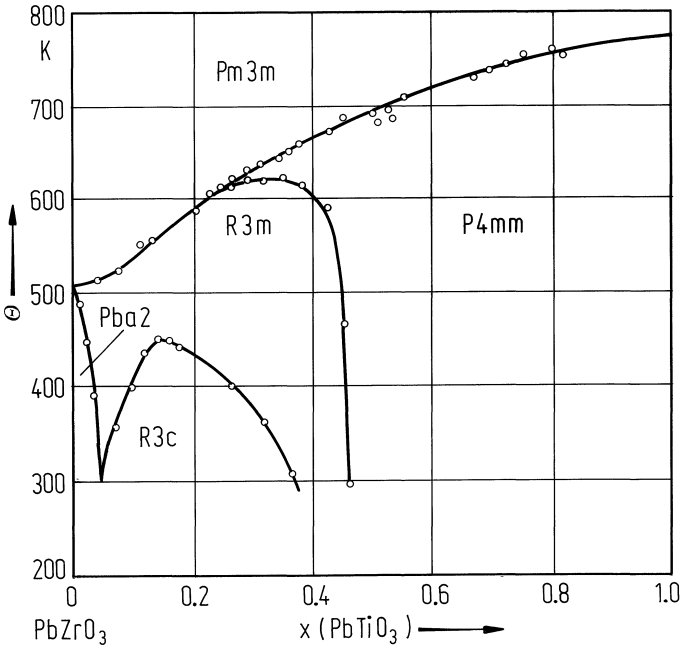

Fig. 1C-a62-004. $Pb(Zr_{1-x}Ti_x)O_3$. Θ vs. x [86Fes].

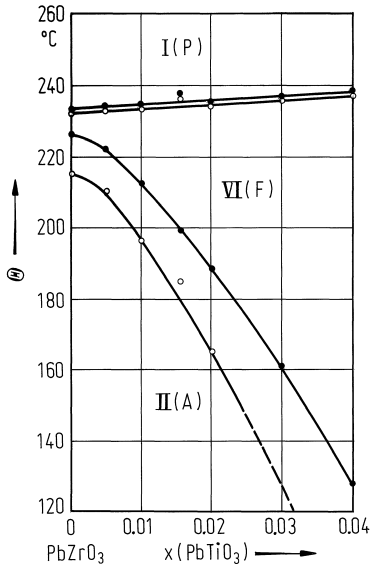

Fig. 1C-a62-005. $Pb(Zr_{1-x}Ti_x)O_3$. Θ vs. x [80Han]. Open circles: on cooling, full circles: on heating.

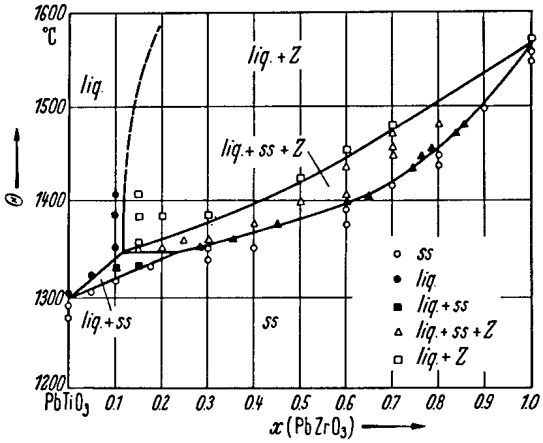

Fig. 1C-a62-006. $Pb(Ti_{1-x}Zr_x)O_3$. Phase diagram [67Fus]. A *c*-*T* section (through $PbTiO_3$–$PbZrO_3$) of ternary PbO–TiO_2–ZrO_2 system. ss: Pb(Zr, Ti)O_3 solid solution, Z: ZrO_2 phase.

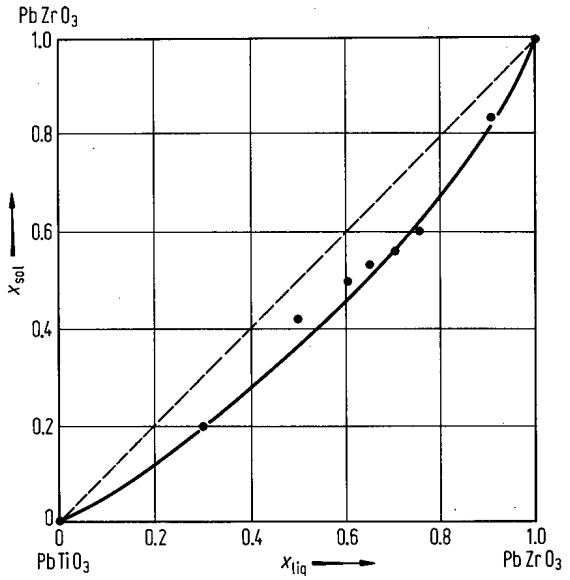

Fig. 1C-a62-007. $Pb(Ti_{1-x}Zr_x)O_3$. x_{sol} vs. x_{liq} [69Tsu]. x_{sol}: composition in solid phase (crystal), x_{liq}: composition in liquid phase (flux solution). Flux: a mixture of KF : PbF_2 : $Pb_3(PO_4)_2$ = 4 : 5.6 : 0.4. For conditions, see original paper.

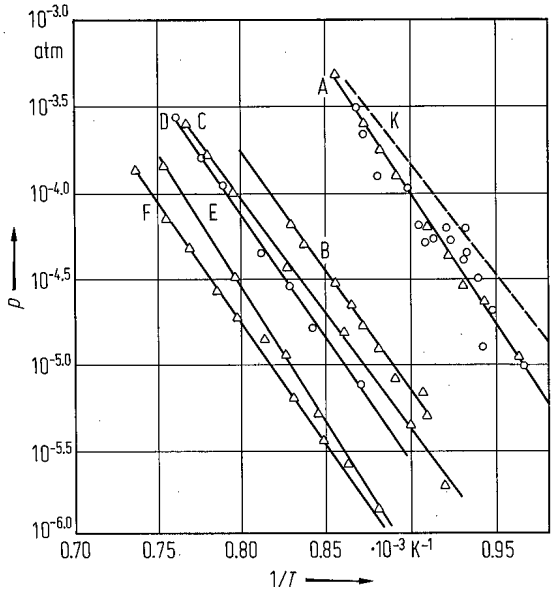

Fig. 1C-a62-008. $Pb(Ti_{1-x}Zr_x)O_3$. p(PbO) vs. $1/T$ [69Har]. p(PbO): vapor pressure of PbO in atm. Curve A: solid PbO, B: x = 1.00, C: x = 0.75, D: x = 0.55, E: x = 0.25, F: x = 0. Dashed curve K: solid PbO after Kubaschewski. Full circles: solid PbO after Nesmeyanow. 1 atm = 101325 Pa.

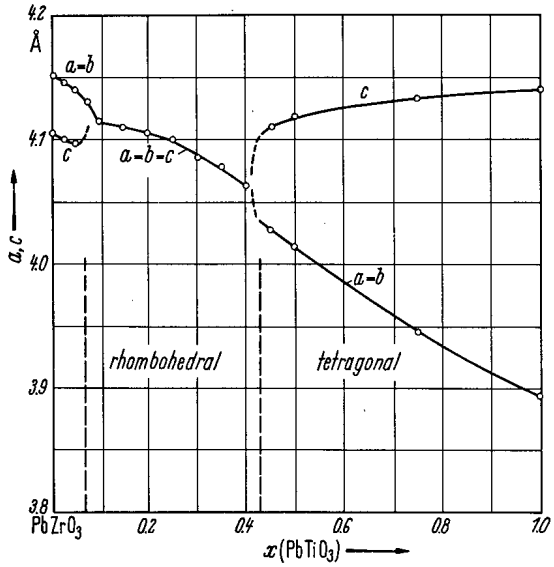

Fig. 1C-a62-009. $Pb(Zr_{1-x}Ti_x)O_3$. *a*, *c* vs. x [52Shi1].

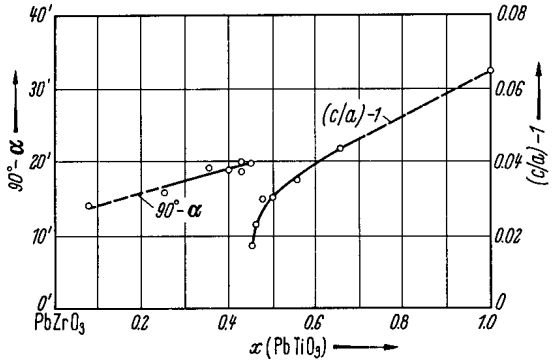

Fig. 1C-a62-010. $Pb(Zr_{1-x}Ti_x)O_3$. $(c/a) - 1$, $90^\circ - \alpha$ vs. x [53Saw].

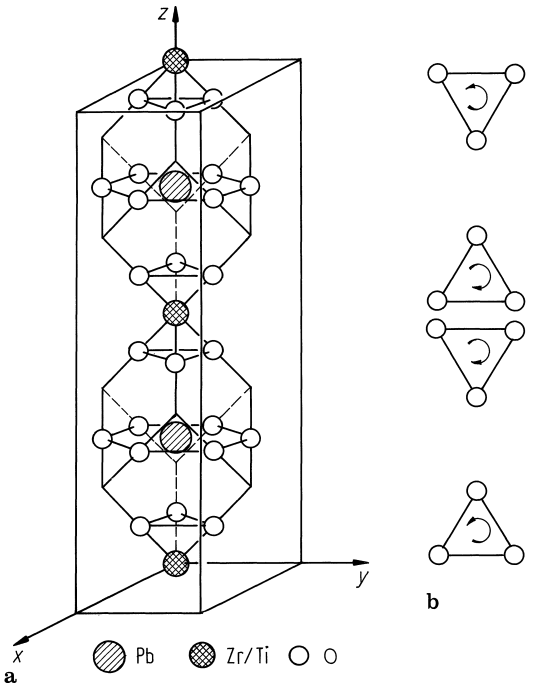

Fig. 1C-a62-011. $Pb(Zr_{0.9}Ti_{0.1})O_3$. **(a)** Arrangement and shift in the unit cell, **(b)** triangles formed by three O atoms of oxygen octahedron viewed along *c*-axis [83Ito].

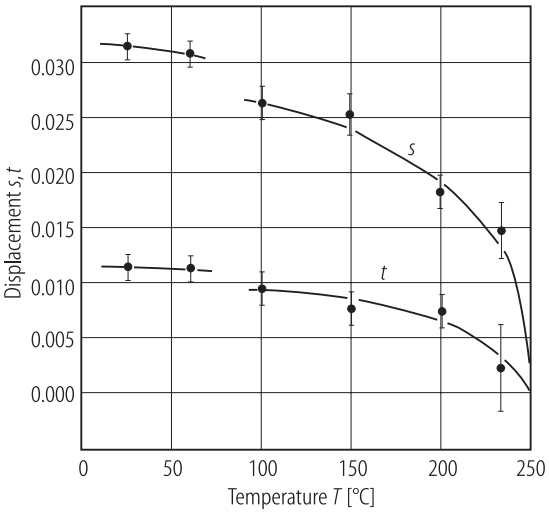

Fig. 1C-a62-012. $Pb(Zr_{0.9}Ti_{0.1})O_3$. *s*, *t* vs. *T* [78Gla]. *s*, *t*: fractional displacement of Pb and Zr/Ti along *c*-axis; see Table 1C-a62-002.

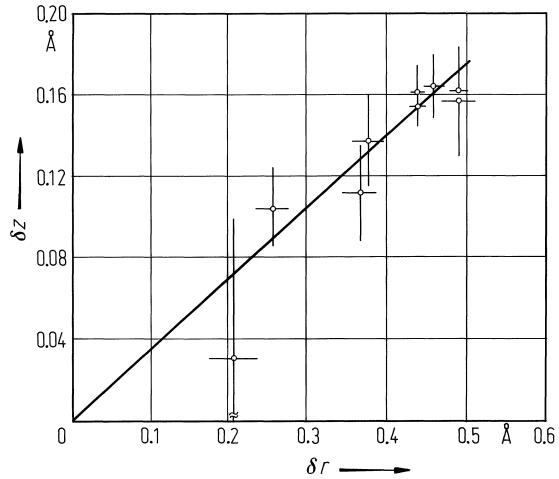

Fig. 1C-a62-013. $Pb(Zr_{1-x}Ti_x)O_3$. δz vs. δr [80Ami]. δz: shift of Zr/Ti, δr: shift of Pb.

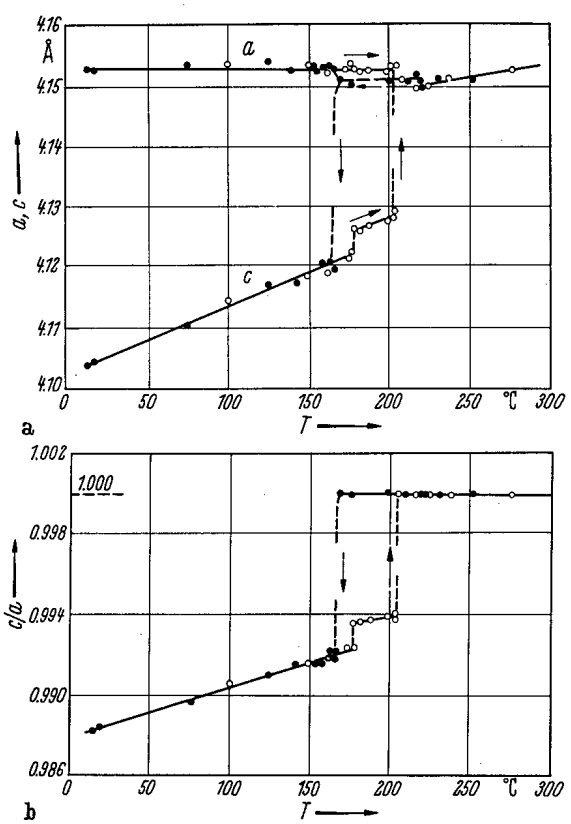

Fig. 1C-a62-014. $Pb(Zr_{0.97}Ti_{0.03})O_3$. Lattice parameters vs. *T* [53Saw]. Open circles: heating, full circles: cooling.

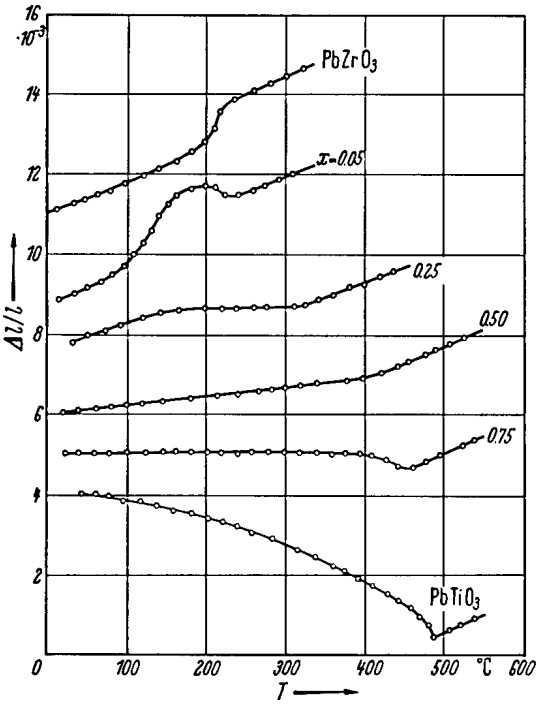

Fig. 1C-a62-015. $Pb(Zr_{1-x}Ti_x)O_3$. $\Delta l/l$ vs. T [52Shi2]. Parameter: x.

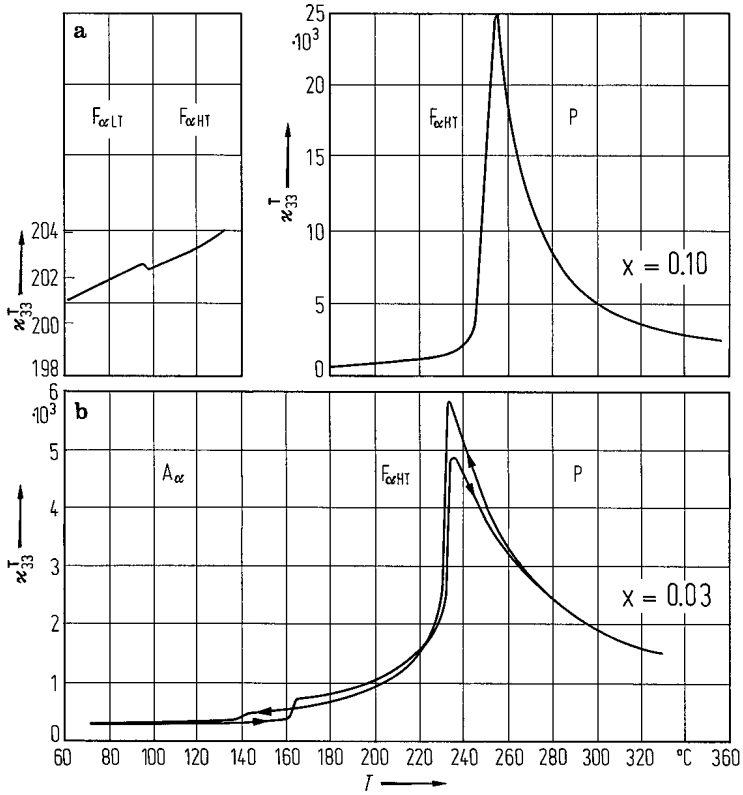

Fig. 1C-a62-016. $Pb(Zr_{1-x}Ti_x)O_3$. κ_{33}^T vs. T [76Cla]. **(a)** x= 0.10, **(b)** x = 0.03.

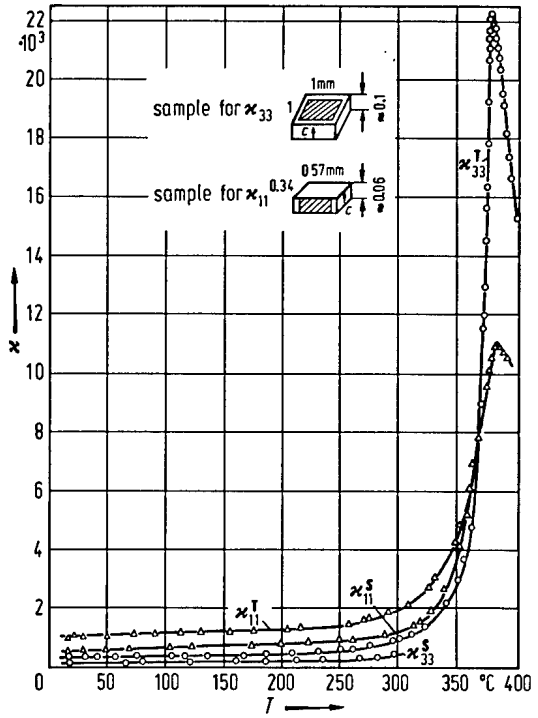

Fig. 1C-a62-017. $Pb(Zr_{0.5}Ti_{0.5})O_3$. κ vs. T [71Tsu]. f = 1 kHz for κ^T, f = 50 MHz for κ^S. (The reason is not known why κ_{33}^T differs from κ_{11}^T above Θ_f.)

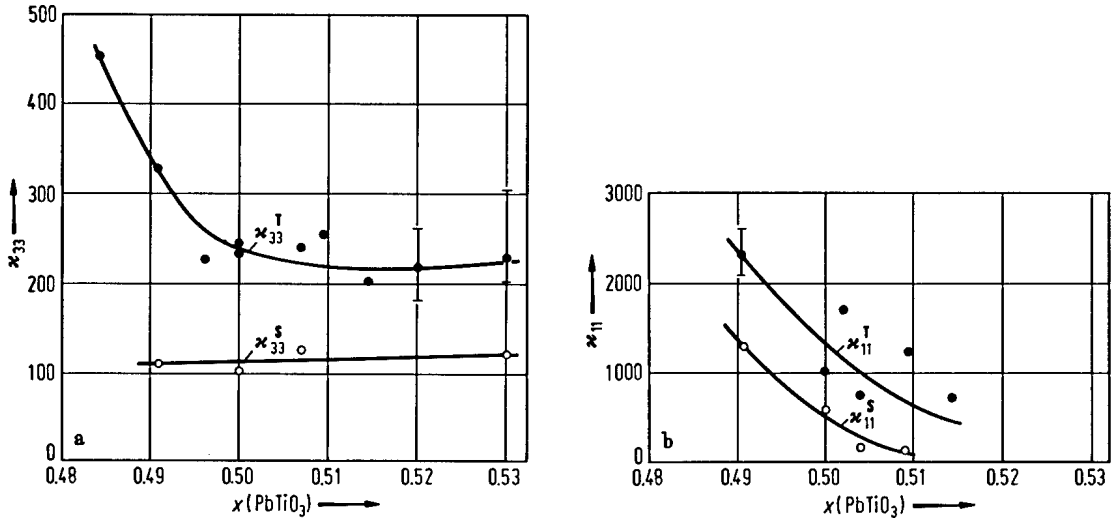

Fig. 1C-a62-018. $Pb(Zr_{1-x}Ti_x)O_3$. κ_{33}^{T}, κ_{33}^{S}, κ_{11}^{T}, κ_{11}^{S} vs. x [74Tsu]. f = 1 kHz for κ^{T}, f = 50 MHz for κ^{S}.

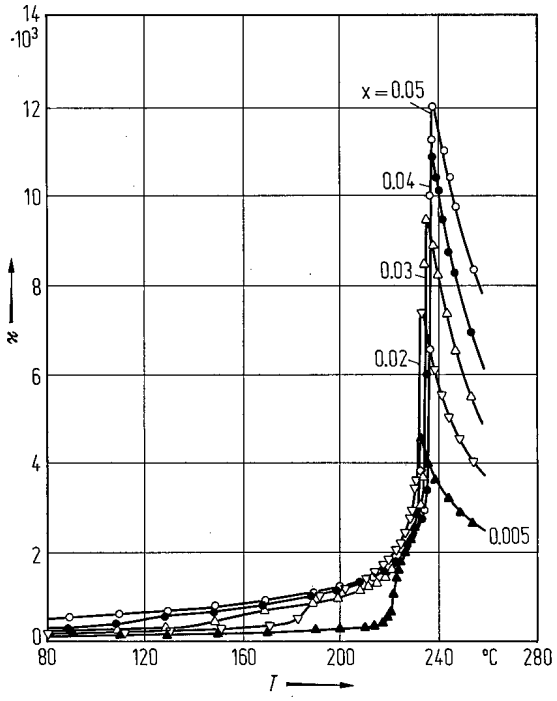

Fig. 1C-a62-019. $Pb(Zr_{1-x}Ti_x)O_3$ (ceramics). κ vs. T [77Han]. Parameter: x. f = 1 MHz.

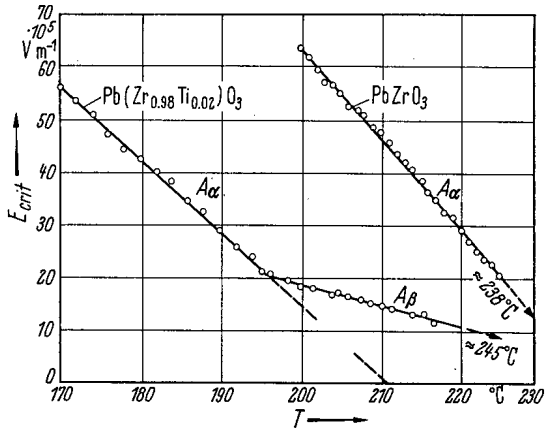

Fig. 1C-a62-020. $PbZrO_3$ and $Pb(Zr_{0.98}Ti_{0.02})O_3$ (ceramics). E_{crit} vs. T [53Saw].

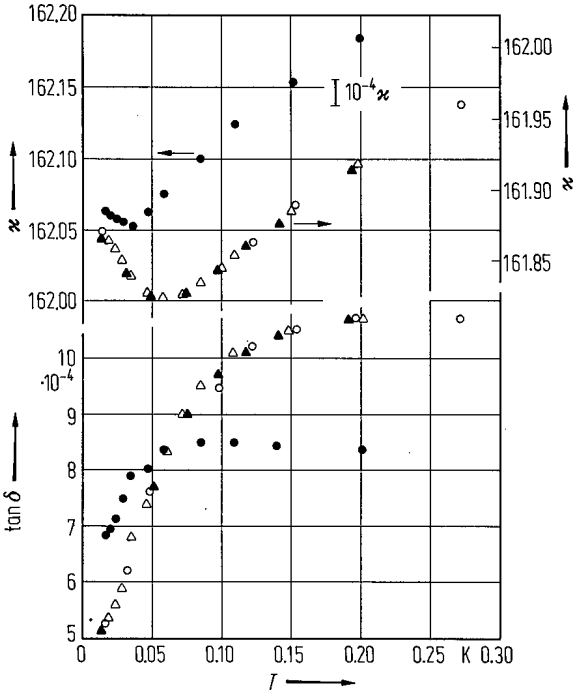

Fig. 1C-a62-021. $Pb(Zr_{0.65}Ti_{0.35})O_3$. κ, $\tan\delta$ vs. T [76Hol]. Parameter: f, E_{bias}. Full circles: f = 0.2 kHz, E_{bias} = 0; open triangles: 10 kHz, 0; open circles: 10 kHz, $1.2 \cdot 10^5$ V m^{-1}; full triangles: 10 kHz, $4.1 \cdot 10^5$ V m^{-1}.

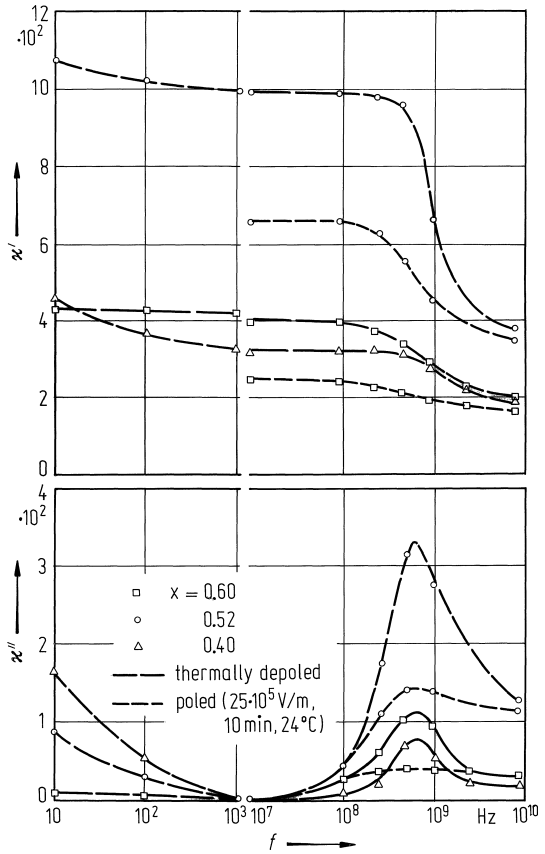

Fig. 1C-a62-022. $Pb(Ti_{1-x}Zr_x)O_3$ (ceramics). κ', κ'' vs. f [86Ker]. Parameter: x.

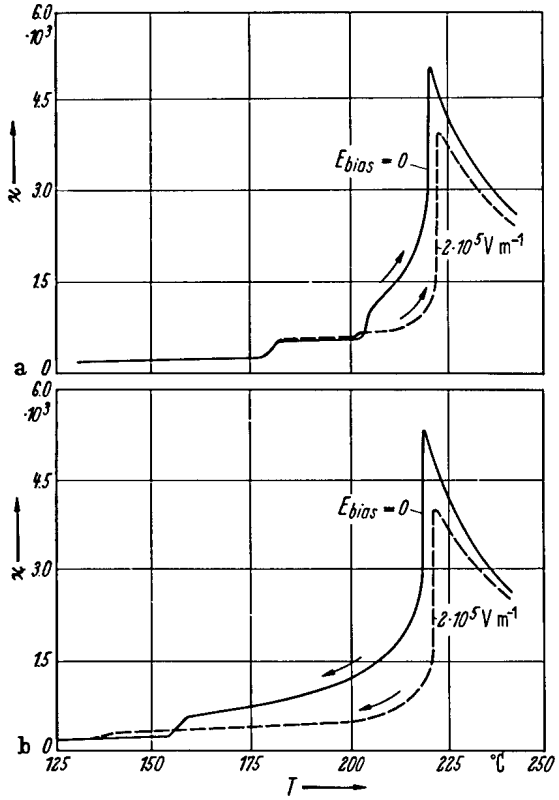

Fig. 1C-a62-023. $Pb(Zr_{0.97}Ti_{0.03})O_3$ (ceramics). κ vs. T [53Saw]. Parameter: E_{bias}. **(a)** heating, **(b)** cooling. f = 1 MHz.

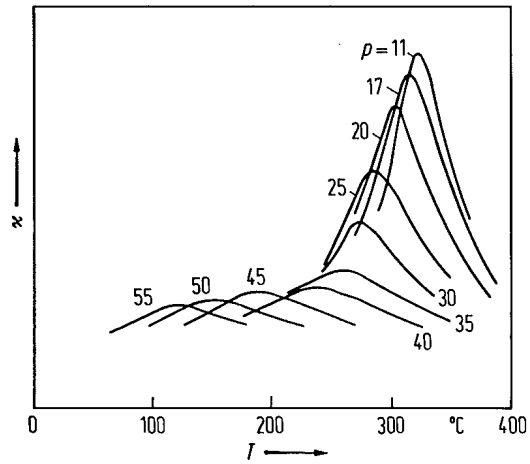

Fig. 1C-a62-024. $Pb(Zr_{0.51}Ti_{0.49})O_3$ (ceramics). κ vs. T [77Hay]. Parameter: p. f = 10 kHz.

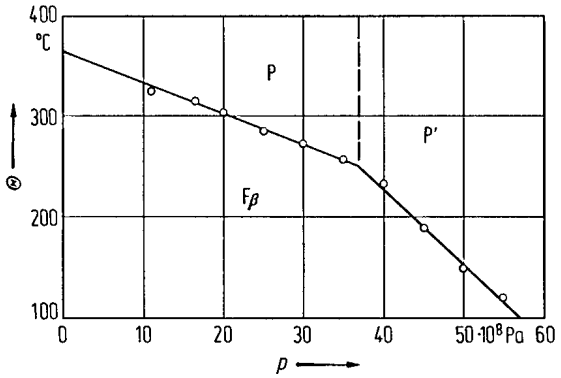

Fig. 1C-a62-025. $Pb(Zr_{0.51}Ti_{0.49})O_3$. Θ vs. p [77Hay].

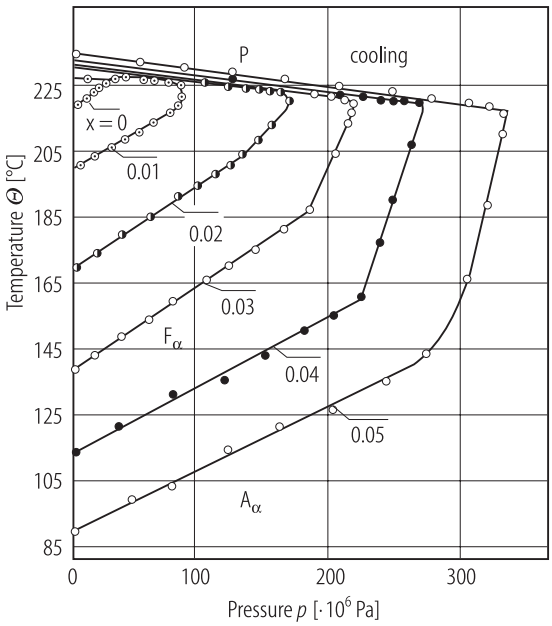

Fig. 1C-a62-026. $Pb(Zr_{1-x}Ti_x)O_3$ (ceramics). Θ vs. p [88Pis]. Parameter: x.

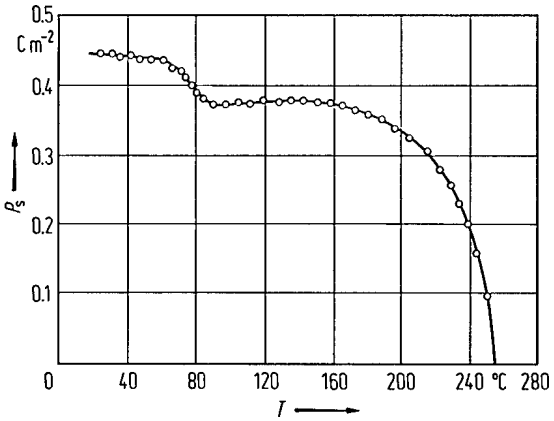

Fig. 1C-a62-027. $Pb(Zr_{0.91}Ti_{0.09})O_3$. P_s vs. T [76Cla].

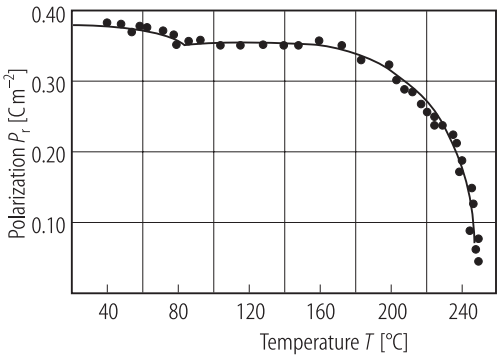

Fig. 1C-a62-028. $Pb(Zr_{0.90}Ti_{0.10})O_3$. P_r vs. T [78Wha]. Crystal was grown from PbO flux.

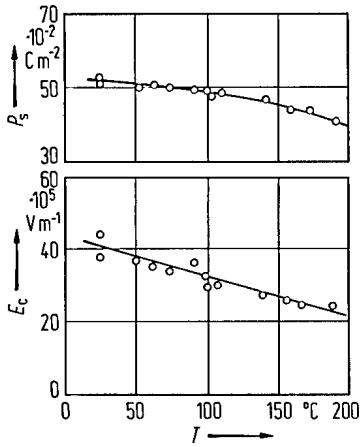

Fig. 1C-a62-029. $Pb(Zr_{0.4}Ti_{0.6})O_3$. P_s, E_c vs. T [74Tsu].

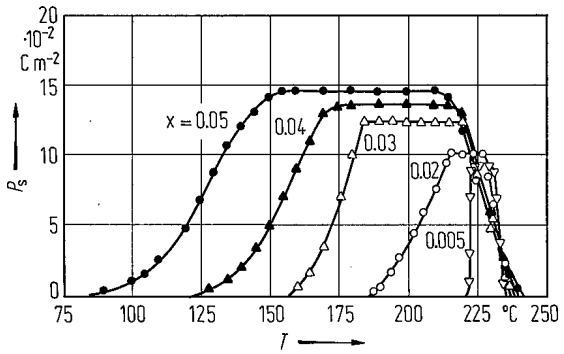

Fig. 1C-a62-030. $Pb(Zr_{1-x}Ti_x)O_3$ (ceramics). P_s vs. T [77Han]. Parameter: x.

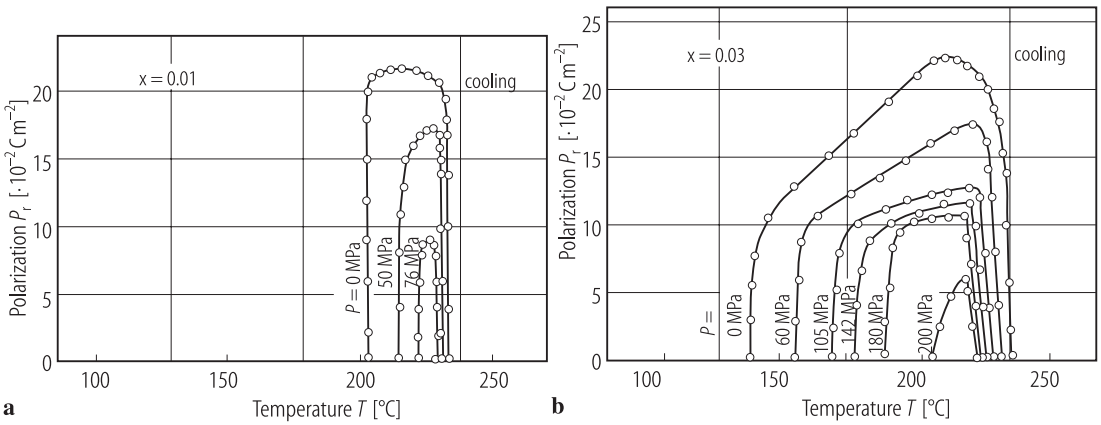

Fig. 1C-a62-031. $Pb(Zr_{1-x}Ti_x)O_3$ (ceramics). P_r vs. T [88Pis]. Parameter: p. **(a)** x = 0.01, **(b)** x = 0.03.

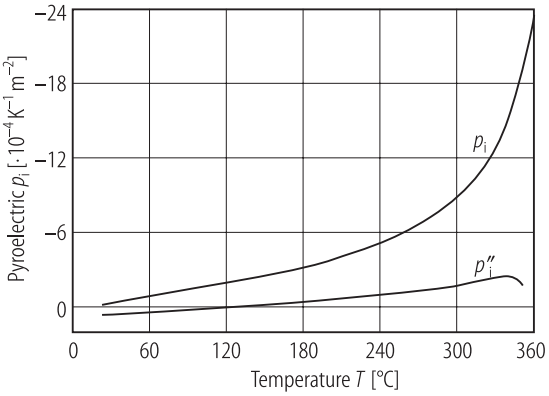

Fig. 1C-a62-032. $Pb(Zr_{0.52}Ti_{0.48})O_3$ (ceramics). p_i, p_i'' vs. T [63Coo]. p_i: primary pyroelectric coefficient, p_i'': secondary pyroelectric coefficient.

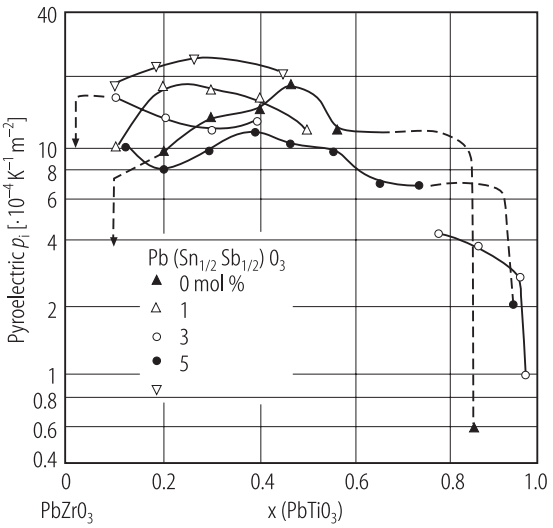

Fig. 1C-a62-033. $Pb(Zr_{1-x}Ti_x)O_3$ (ceramics). p_i vs. x [82Mur]. Parameter: content of additive $Pb(Sn_{1/2}Sb_{1/2})O_3$ in mol %. p_i: pyroelectric coefficient.

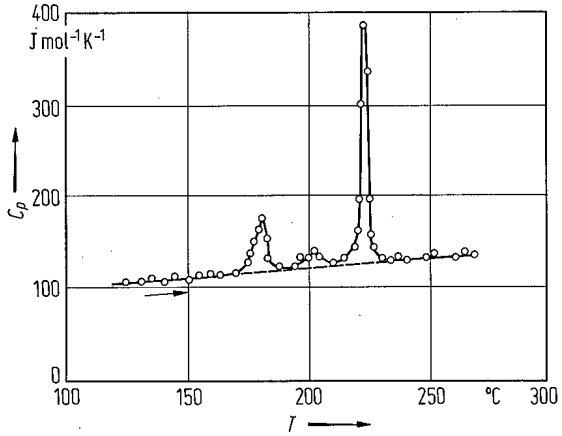

Fig. 1C-a62-034. $Pb(Zr_{0.97}Ti_{0.03})O_3$. C_p vs. T [53Saw].

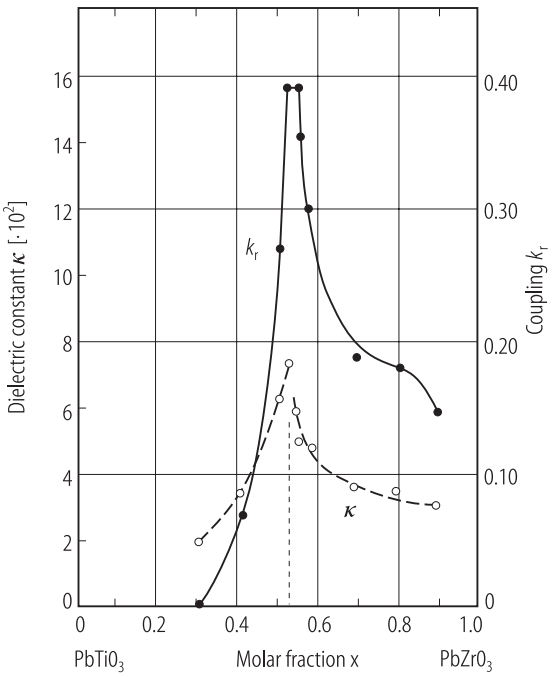

Fig. 1C-a62-035. $Pb(Ti_{1-x}Zr_x)O_3$ (ceramics). κ , k_r vs. x [55Jaf] (classical data). κ: dielectric constant at 25 °C, f = 1 MHz; k_r: radial coupling factor at 25 °C.

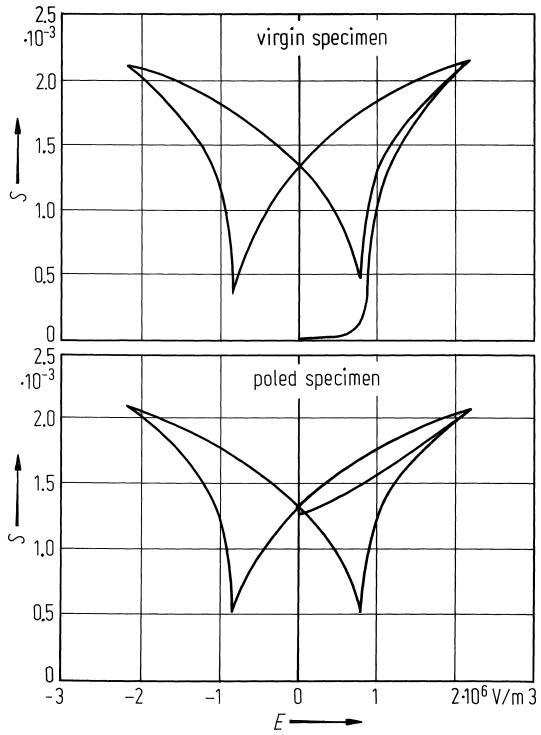

Fig. 1C-a62-036. $Pb(Zr_{0.65}Ti_{0.35})O_3$ (ceramics). *S* vs. *E* [81Che]. *S*: strain, *E*: electric field.

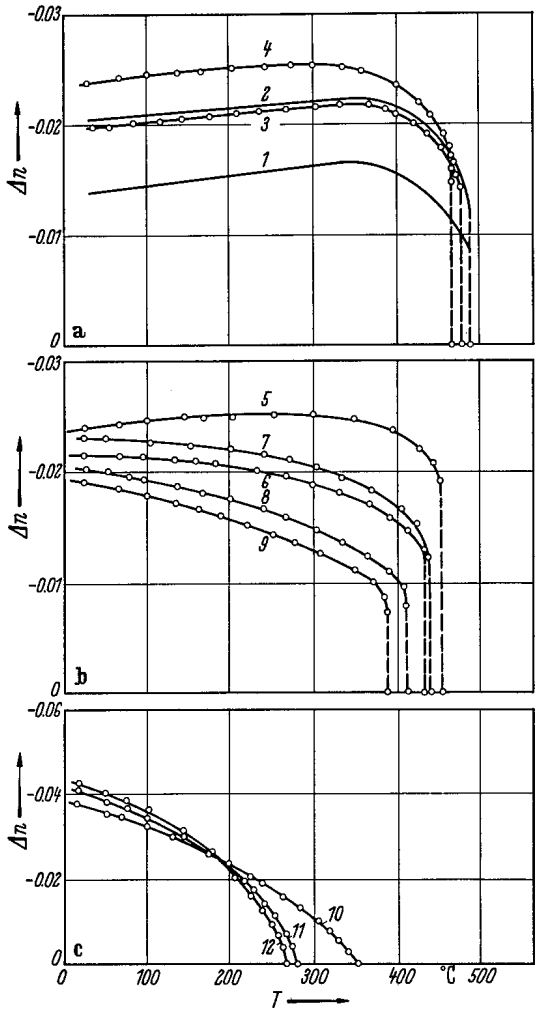

Fig. 1C-a62-037. $Pb(Ti_{1-x}Zr_x)O_3$. Δn vs. T [65Fus]. Parameter: x. Δn: birefringence. Light source: Xe lamp except for *1* and *2* (after [59Kob]). Curve *1*: x = 0 (λ =500 nm), *2*: 0 (λ = 450 nm), *3*: 0.10, *4*: 0.15, *5*: 0.20, *6,7*: 0.30, *8*: 0.40, *9*: 0.50, *10:* 0.60, *11*: 0.80, *12*: 0.85.

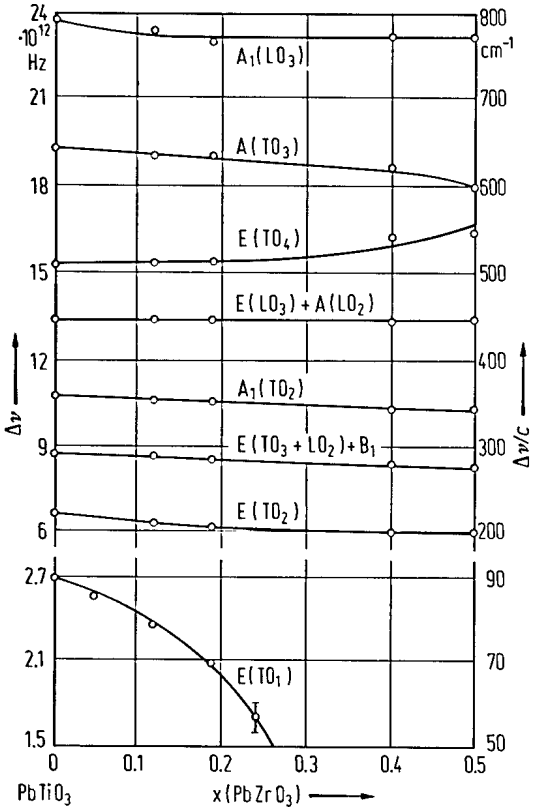

Fig. 1C-a62-038. $Pb(Ti_{1-x}Zr_x)O_3$. $\Delta\nu$ vs. x [70Bur]. $\Delta\nu$: Raman frequency shift (powdered specimen at 23 °C).

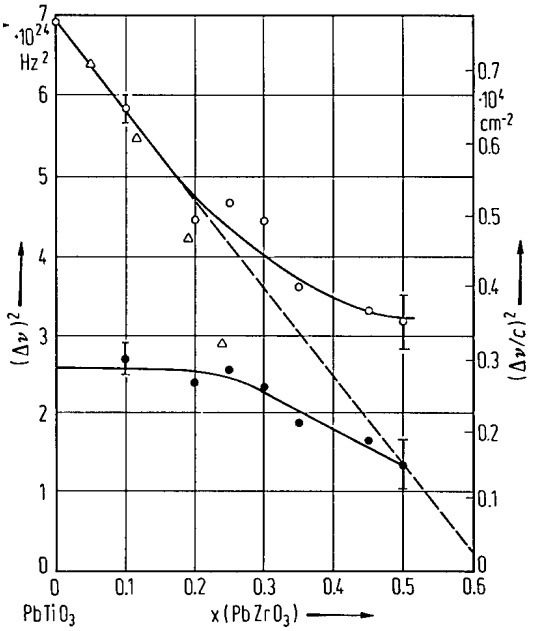

Fig. 1C-a62-039. $Pb(Ti_{1-x}Zr_x)O_3$. $(\Delta\nu)^2$ vs. x [74Bau]. $\Delta\nu$: Raman frequency shift of powdered specimen at 295 K. Triangles: results after [70Bur], open circles: lowest E(TO) mode, full circles: unknown mode. The broken line is extrapolation from the upper curve at x = 0.

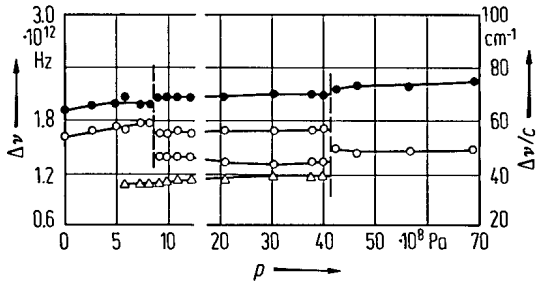

Fig. 1C-a62-040. $Pb(Zr_{0.9}Ti_{0.1})O_3$ (ceramics). $\Delta\nu$ vs. p [77Bau]. $\Delta\nu$: Raman frequency shift at 300 K. For explanation of symbols see [77Bau].

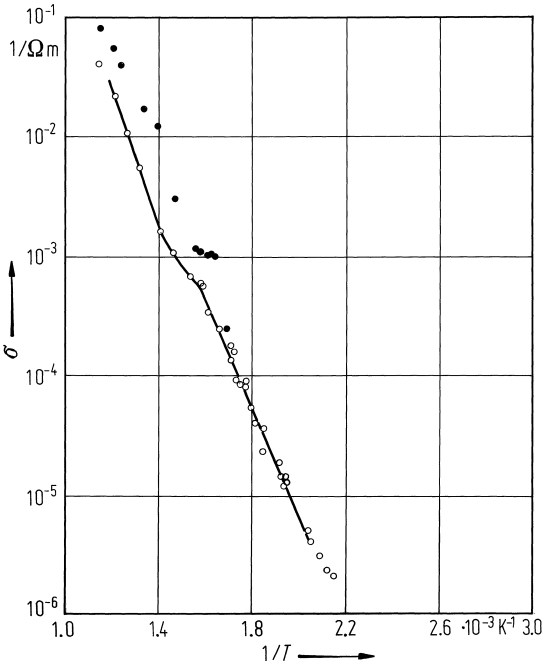

Fig. 1C-a62-041. $Pb(Zr_{0.65}Ti_{0.35})O_3$ (ceramics). σ vs. $1/T$ [82Sch]. σ: conductivity at partial pressure of O_2 of 50 Pa (open circles) and 3.5 kPa (full circles).

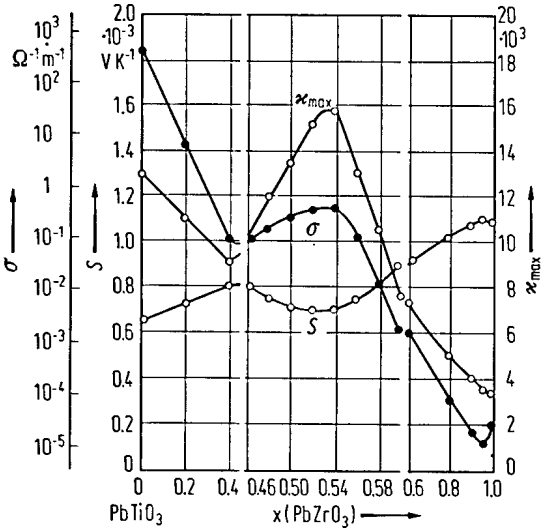

Fig. 1C-a62-042. Pb($Ti_{1-x}Zr_x$)O_3 (ceramics). σ, S, κ_{max} vs. x [78Wro]. $T = \Theta_f$. σ: electrical conductivity, S: Seebeck coefficient, κ_{max}: maximum dielectric constant.

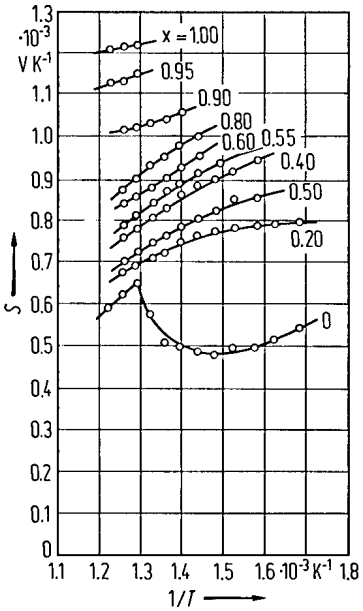

Fig. 1C-a62-043. $Pb(Ti_{1-x}Zr_x)O_3$ (ceramics). *S* vs. 1/*T* [78Dud]. Parameter: x. *S*: Seebeck coefficient.

References

52Shi1 Shirane, G., Suzuki, K.: J. Phys. Soc. Jpn. **7** (1952) 333.
52Shi2 Shirane, G., Suzuki, K., Takeda, A.: J. Phys. Soc. Jpn. **7** (1952) 12.
52Shi3 Shirane, G., Takeda, A.: J. Phys. Soc. Jpn. **7** (1952) 5.
53Saw Sawaguchi, E.: J. Phys. Soc. Jpn. **8** (1953) 615.
55Jaf Jaffe, B., Roth, R.S., Marzullo, S.: J. Res. Natl. Bur. Stand., Sect. A **55** (1955) 239.
59Kob Kobayashi, J., Yamada, N.: Mem. Sch. Sci. Eng., Waseda Univ. **23** (1959) 111.
62Bar Barnett, H.M.: J. Appl. Phys. **33** (1962) 1606.
62Ike Ikeda, T., Fushimi, S.: J. Phys. Soc. Jpn. **17** (1962) 1202.
63Coo Cook Jr., W.R., Berlincourt, D.A., Scholz, F.J.: J. Appl. Phys. **34** (1963) 1392; erratum: **34** (1963) 3154.
64Fus Fushimi, S., Ikeda, T.: Jpn. J. Appl. Phys. **3** (1964) 171.
65Fus Fushimi, S., Ikeda, T.: J. Phys. Soc. Jpn. **20** (1965) 2007.
65Glo Glower, D.D., Hester, D.L., Warnke, D.F.: J. Am. Ceram. Soc. **48** (1965) 417.
66Ber Berlincourt, D.: IEEE Trans. Sonics Ultrason. **SU-13** (1966) 116.
67Fus Fushimi, S., Ikeda, T.: J. Am. Ceram. Soc. **50** (1967) 129.
69Har Hardtl, K.H., Rau, H.: Solid State Commun. **7** (1969) 41.
69Mic Michel, C., Moreau, J.M., Achenbach, G.D., Gerson, R., James, W.J.: Solid State Commun. **7** (1969) 865.
69Tsu Tsuzuki, K., Sakata, K., Wada, M.: Jpn. J. Appl. Phys. **8** (1969) 816.
70Bur Burns, G., Scott, B.A.: Phys. Rev. Lett. **25** (1970) 1191.
71Bar Barsukova, M.L., Kuznetsov, V.A., Lobachev, A.N., Lider, V.V.: Kristallografiya **16** (1971) 222; Sov. Phys. Crystallogr. (English Transl.) **16** (1971) 178.
71Tsu Tsuzuki, K.: Doctor Thesis, Tohoku University, 1971.
73Lan Lane, R., Lufl, D., Brown, K.R., Marshallsay, H.J.: Trans. J. Brit. Ceram. Soc. **72** (1973) 39.
74Bau Bauerle, D., Yacoby, Y., Richter, W.: Solid State Commun. **14** (1974) 1137.
74Cla Clarke, R., Glazer, A.M.: J. Phys. C **7** (1974) 2147.
74Ede Edelglass, S.M., Lendvai-Lintner, E.: Phys. Status Solidi (a) **25** (1974) K155.
74Mer Merlin, R., Pinczuk, A.: Ferroelectrics **7** (1974) 275.
74Tsu Tsuzuki, K., Sakata, K., Wada, M.: Ferroelectrics **8** (1974) 501.
75Mer Merlin, R., Sanjurjo, J.A., Pinczuk, A.: Solid State Commun. **16** (1975) 931.
76Cla Clarke, R., Whatmore, R.W.: J. Cryst. Growth **33** (1976) 29.
76Hol Holste, J.C., Lawless, W.N., Samara, G.A.: Ferroelectrics **11** (1976) 337.
76Mer Merlin, R., Sanjurjo, J.A., Pinczuk, A.: Proc. Int. Conf. Light Scattering Solids, 3rd, held in Campinas, Brazil (1975), Balinski, M., Leite, R.C.C., Porto, S.P.S. (eds.), Flammarion Sciences, 1976, p. 895.
77Bau Bauerle, D., Holtzapfel, W.B., Pinczuk, A., Yacoby, Y.: Phys. Status Solidi (b) **83** (1977) 99.
77Han Handerek, J., Ujma, Z.: Acta Phys. Polon. **A51** (1977) 87.
77Hay Hayashi, M., Hasegawa, K., Hayashi, K.: Jpn. J. Appl. Phys. **16** (1977) 505.
78Dud Dudek, J., Wrobol, Z.: Ferroelectrics **18** (1978) 161.
78Gla Glazer, A.M., Mabud, S.A., Clarke, R.: Acta Crystallogr., Sect. B **34** (1978) 1060.
78Wha Whatmore, R.W., Clarke, R., Glazer, A.M.: J. Phys. C **11** (1978) 3089.
78Wro Wrobel, Z.: Phys. Status Solidi (a) **45** (1978) K67.
79Cas Castellano, R.N., Feinstein, L.G.: J. Appl. Phys. **50** (1979) 4406.
79Ham1 Hamada, H., Ohshika, T., Hirai, H.: Oyo Buturi **48** (1979) 602.
79Ham2 Hamada, H., Ohshika, T., Hirai, H.: Trans. Inst. Electron. Commun. Eng. Jpn. **62C** (1979) 464.
80Ami Amin, A., Newnham, R.E., Cross, L.E.: Mater. Res. Bull. **15** (1980) 721.
80Han Handerek, J., Ujma, Z., Roleder, K.: Phase Transitions **1** (1980) 377.
81Che Chen, P.J., Tucker, T.J.: Acta. Mech. **38** (1981) 209.

82Mur Murata, M., Ito, S.: Proc. 2nd Sensor Symposium, Tsukuba, May 1982 (The Institute of Electrical Engineers of Japan, Tokyo, 1982), p. 4547.
82Sch Schwitzgebel, G., Maier, J., Wicke, U., Schmitt, H.: Z. Phys. Chem., N. F. **130** (1982) 97.
83Bar Barbulescu, A., Barbulescu, E., Barb, D.: Ferroelectrics **47** (1983) 221.
83Fuk Fukami, T., Sakuma, T., Tokunaga, K., Tsuchiya, H.: Jpn. J. Appl. Phys. **22**, Suppl. 22-2 (1983) 18.
83Ito Ito, H., Shiozaki, Y., Sawaguchi, E.: J. Phys. Soc. Jpn. **52** (1983) 913.
84Fuk Fukushima, J., Kodaira, K., Matsushita, T.: J. Mater. Sci. **19** (1984) 595.
84Kut Kutty, T.R.N., Balachandran, R.: Mater. Res. Bull. **19** (1984) 1479.
84Zor Zorn, G.: Ferroelectrics **55** (1984) 91.
85Cha Chang, Y.-J., Lian, J.-Y., Wang, Y.-l.: Appl. Phys. **A36** (1985) 221.
85FuS Fu, S.-L., Chung, J.K., Cheng, S.Y.: Jpn. J. Appl. Phys. **24**, Suppl. 24-2 (1985) 416.
85Han Handerek, J., Kwapulinski, J., Pawelczyk, M., Ujma, Z.: Phase Transitions **6** (1985) 35.
85NgY Ng, Y.S., McDonald, A.D.: Ferroelectrics **62** (1985) 167.
86Fes Fesenko, E.G., Eremkin, V.V., Smotrakov, V.G.: Fiz. Tverd. Tela **28** (1986) 324; Sov. Phys. Solid State (English Transl.) **28** (1986) 181.
86Ker Kersten, O., Schmidt, G.: Ferroelectrics **67** (1986) 191.
86Pol Polandov, I.N., Gulish, O.K., Alekhina, N.S., Isaev, G.P., Malyutin, B.I., Kalinin, V.I.: Izv. Akad. Nauk SSSR, Neorg. Mater. **22** (1986) 262; Inorg. Mater. (English Transl.) **22** (1986) 222.
88Pis Pisarski, M., Dmytrow, D.: Ferroelectrics **77** (1988) 121.
90Ekn Eknadiosiants, E.I., Borodin, V.Z., Smotrakov, V.G., Eremkin, V.V., Pinskaya, A.N.: Ferroelectrics **111** (1990) 283.
90Gli Glinchuk, M.D., Bykov, I.P., Kurliand, V.M., Boudys, M., Kala, T., Nejezchlev, K.: Phys. Status Solidi (a) **122** (1990) 341.
92Byk Bykov, I.P., Glinchuk, M.D., Skorokhod, V.V., Kurland, V.M., Boudys, M., Kala, T.: Ferroelectrics **127** (1992) 89.
92Hat Hatanaka, T., Hasegawa, H.: Jpn. J. Appl. Phys. **31** (1992) 3245.
93War Warren, W.L., Tuttle, B.A., Schwartz, R.W., Hammetter, W.F., Goodnow, D.C., Evans, J.T., Bullington, J.A.: Mater. Res. Soc. Symp. Proc. **310** (1993) 3.
94AlS Al-Shareef, H.N., Bellur, K.R., Auchiello, O., Chen, X., Kingon, A.I.: Thin Solid Films **252** (1994) 38.